RSC Advances

Facile Synthesis of High-surface-area Activated Carbon from Coal for Supercapacitor and High CO2 Sorption

Journal:	*RSC Advances*
Manuscript ID	RA-ART-12-2015-026044.R1
Article Type:	Paper
Date Submitted by the Author:	03-Apr-2016
Complete List of Authors:	Chu, Wei; Sichuan University (Top 12th Univ in China), Dept Chemical Engineering Peng, Zhu; Sichuan University, Department of Chemical Engineering Guo, Zhanglong; Sichuan University (Top 12th Univ in China), Dept Chemical Engineering Wei, Min ; Sichuan University (Top 12th Univ in China), Dept Chemical Engineering
Subject area & keyword:	Carbon materials < Materials

RSC Advance

ARTICLE

Facile Synthesis of High-surface-area Activated Carbon from Coal for Supercapacitor and High CO_2 Sorption†

Received 00th January 20xx,
Accepted 00th January 20xx

DOI: 10.1039/x0xx00000x

www.rsc.org/

Zhu Peng , Zhanglong Guo , Wei Chu *, Min Wei

Carbon materials have attracted much attention in many applications. Herein, high performance activated carbons (ACs) were synthesized from cheap coal raw material via facile strategy by KOH activation. AC4T800t2 exhibited the higher BET surface area (2457 m^2 g^{-1}) and larger total pore volume (1.448 cm^3 g^{-1}) among the as-synthesized ACs samples. The optimized material (AC4T800t2) displayed the specific capacitance as high as 384 F g^{-1} at the scan rate of 5 mV s^{-1} in 6 M KOH. The capacitance retained still 279 F g^{-1}, even at a high scan rate of 200 mV s^{-1}, showing good rate performance. AC4T800t2 also showed excellent cycle performance (95% retention capacity after 5000 cycles) at the current density of 5 A g^{-1}. Furthermore, these ACs samples for CO_2 sorption were also investigated using a pressure swing adsorption (PSA) process. The CO_2 sorption behaviors of these samples were tested at 298.15 K in pressure range of 0–1 MPa by volumetric method. The Langmuir model provided good agreement with the experimental data (correlation coefficient above 0.99). The optimized material (AC4T800t2) showed high CO_2 sorption capacity of 169.44 mL g^{-1} (7.56 mmol g^{-1}) at 1 MPa, also high CO_2 saturated uptake of 20.81mmol g^{-1} (91.56 wt%). Better CO_2 uptake is dependent on larger micropore volume and higher specific surface area. In brief, the high performance AC samples have been synthesized for supercapacitor and CO_2 sorption.

1. Introduction

Nowadays, the increasing demand for energy and rising global greenhouse gas emissions has motivated intense research to look for eco-friendly and alternative energy resources.[1] Carbon materials have received considerable attention in gas storage[2], catalyst support[3], and electrode materials[4] because of their high surface area, fine electrical conductivity, proper pore size distribution (PSD), remarkable physical–chemical stability, low cost and easy preparation.[5-7] In particular, ACs are the most commonly used materials because of their high surface area (>1000 m^2 g^{-1}), big pore volume (>0.5 cm^3 g^{-1}), facile synthesis and relatively low price.[8, 9]

Rich-carbon materials (wood[10], nutshell[11], coal[12], and polymer[13]) are widely used as precursors to manufacture ACs, which is attributed to its availability and cheapness. Among them, coal is the most commonly used material. ACs can be prepared by two different methods: (i) Physical activation with different oxidizing gases (air, O_2, CO_2, steam or their mixtures); (ii) Chemical activation by mixing carbonaceous materials with chemical activating agents (KOH, NaOH, H_3PO_4, H_2SO_4, $ZnCl_2$, $FeCl_3$, K_2CO_3 or other chemical compounds).[8, 11, 14] In comparison to the physical activation, chemical activation presents several advantages: lower activation temperature, shorter activation time, higher product yield, more well-developed microporosity, and higher surface area.[8, 15-17] Among various chemical reagents, KOH is the most effective agent to obtain a microporous carbon material with narrow PSD and high surface area.[16, 18, 19] The characteristics of ACs are influenced by the type of raw materials, activation agent/precursor ratio, method of mixing, activation temperature, activation time, heating rate, gas flow rate, and washing stage conditions et al.[20-22] Physical mixing requires less time and work than the other methods of mixing.[23] By optimizing the preparation conditions, the high performance ACs can be developed, and applied to the supercapacitor and CO_2 sorption.

The supercapacitors are promising candidates for high energy storage due to their higher power density, longer cycle life, faster charge/discharge processes, and lower maintenance cost, as well as the better safety than secondary batteries, also higher energy density than conventional electrostatic capacitors.[24-26] Carbon-based materials storage energy based on the accumulation of charge in the double layer formed at the surface of inert electrodes.[27] Up to now, various carbon-based materials, such as ACs[28], carbon nanotubes[29], templated porous carbons[7], graphene[30], have been considered as electrode materials for supercapacitors aiming at high special capacitance coupled with high power and energy densities. Especially, ACs remain the first choice of electrode materials for supercapacitors because of their large surface area, high electronic conductivity, easy preparation, good chemical stability and low cost.[12, 31] It has been widely acknowledged that specific surface area, pore size distribution and surface chemistry are of prime importance to the electrochemical properties.[31-33]

The atmospheric CO_2 concentration will reach 550 ppm by 2050 from 384 ppm in 2007 on condition that CO_2 emission is stable for the next four decades.[34, 35] The atmospheric CO_2 accumulation which is mainly caused by fossil fuel combustion is considered as a main contributor to global warming in the past century.[35] In recent years, great efforts have been directed towards developing various technologies for CO_2 capture, usage and storage (CCUS)[36], including adopting liquids, solids and membranes as adsorbents.[37] Pressure swing adsorption (PSA) technology has gained much attention due

Department of Chemical Engineering, Sichuan University, Chengdu 610065 (China).E-mail: chuwei1965@scu.edu.cn

†Electronic Supplementary Information (ESI) available: [details of any supplementary information available should be included here]. See DOI: 10.1039/x0xx00000x

to low energy requirements and low capital investment.[38] Adsorption between solid adsorbents and CO_2 is receiving increasing attention due to the advantages of low energy requirements for regeneration, great capture capacity, ease of handling, and reduced environmental impact, etc.[39] Of the sorbents applied so far, ACs are proposed as suitable candidates for CO_2 sorption due to their high surface area, easy-to-design pore structure, and stable physicochemical properties.[40-42]

In this paper, the low-cost coal was used as the raw material and activated by KOH agent. The influences of the agent/coal ratio and activation time on the characteristics of the ACs were investigated in detail. A facile activation process was demonstrated for the preparation of ACs. The optimized material (AC4T800t2) exhibited the higher BET specific surface area (2457 m^2 g^{-1}) and larger total pore volume (1.448 cm^3 g^{-1}) among the as-synthesized ACs samples. The material possessed excellent performance of supercapacitor and CO_2 sorption. AC4T800t2 displayed a high capacitance of 384 F g^{-1} at the scan rate of 5 mV s^{-1} in 6 M KOH. The capacitance retained still 279 F g^{-1}, even at a high scan rate of 200 mV s^{-1}. No capacitance decay was almost observed after 5000 cycles at the current density of 5A g^{-1}. The capacitance retention was as high as 95%. The AC4T800t2 symmetric supercapacitor exhibited a maximum energy density of 4.2 W h kg^{-1} with a powder density of 100 W kg^{-1} at the current density of 0.2 A g^{-1} in 6 M KOH. Meanwhile, the use of ACs for the sorption of CO_2 by a PSA process has been researched. The optimized material (AC4T800t2) showed high CO_2 sorption capacity of 169.44 mL g^{-1} (7.56 mmol g^{-1}) at 1 MPa, also high CO_2 saturated uptake of 20.81mmol g^{-1} (91.56 wt%). Such remarkable performances showed that ACs from low-cost coal are promising materials for commercial supercapacitors and CO_2 sorption.

2. Experimental section

2.1 Materials

High rank coals (Hunan Province, China) was used as carbon source. KOH was bought from Chengdu Kelong Chemical Co., Ltd. All other chemical reagents were in analytical grade. Deionized water was used for washing.

2.2 Preparation of activated carbons

Chemical activation of high rank coals was performed using KOH as activating agent. In order to investigate the optimal conditions for producing high surface area ACs, different KOH/coal ratios and activation times were studied in detail. The synthesis process of ACs was shown in Fig. 1. The detailed process was as follows: three grams of dried coal were physically mixed with KOH by high-speed multi-function mill (Shanghai Bingdu Company). In this work, KOH/coal ratios of 2, 3, 4, 5 and 6 were studied. The activation was carried out in a horizontal tubular furnace (Nanjing Nanda Instrument Plant) and the temperature of reactor was increased at the rate of 5°C min^{-1}, until it reached the desired activation temperature. Samples were kept at the activation temperature for different activation time of 1, 1.5, 2, 2.5 and 3h before cooling down under nitrogen flow. The process was performed under nitrogen flow of 100 mL min^{-1}. After activation, the samples were cooled down to room temperature. Subsequently, the resulting products were washed sequentially several times with 5 M HCl, followed by distilled water to remove residual chemicals. Once the residual alkali was completely removed, the sample was dried overnight at 110 °C in an oven. The resultant coal-based ACs were denoted as ACxTytz, where x refers to the KOH/coal ratio, y represents the activation temperature, and z means the activation time.

2.3 Characterization of activated carbons

Fig. 1 Schematic diagram for the synthesis of ACs from coal

The yield was defined as the weight ratio of final AC to the initial dried coal. The pore structure characteristics of the samples were obtained by N_2 adsorption/desorption isotherms at 77 K using a NOVA1000e surface area and pore size analyser (Quantachrome Company). Prior to the analysis, samples were degassed at 473 K in a vacuum condition for 180 min. The BET surface area, micropore volume and pore size distribution of the samples were measured by application of the BET, DK and DFT equation, respectively. The total pore volume was estimated at a relative pressure p/p_0 = 0.98–0.99. Surface morphology was investigated by scanning electron microscopy (SEM). The structure was examined using Raman scattering spectra. The weight change of the samples during heat treatment was determined with a thermo-gravimetric analyser (TGA Q500). Surface functional groups were investigated by Fourier transforms infrared spectrometer (FT-IR, Bruker Tensor, Germany) in the range from 4000 to 400 cm^{-1} and X-ray photoelectron spectroscopy (XPS，AXIS Ultra DLD).

2.4 Electrochemical measurements

All the electrochemical measurements were performed on a CHI-660E electrochemical workstation (Chenhua, Shanghai, China) at ambient temperature. Three-electrode system tests were carried out in 6 M KOH aqueous electrolyte, employing Pt wire as the counter electrode, and Hg/HgO electrode as the reference electrode, respectively. The 80 wt% active material was ground, and then mixed with 10 wt% polyvinylidene fluoride binder and 10wt % carbon black in 5 mL N-methyl-2-pyrrolidone. The working electrode was prepared by coating the mixture on the 1 cm × 3 cm nickel foam. After the electrode materials were loaded, the working electrode was dried at 110 °C for 12 h and then pressed at 10 MPa for 30 s. Each electrode contained 4-5 mg of active materials. All cyclic voltammetry (CV) curves were collected with a potential window from -1 to 0 V at different scan rates from 5 to 200 mV s^{-1}. Galvanostatic charge-discharge cycling (GCD) tests were conducted with different current densities from 0.2 to 10 A g^{-1}. Electrochemical impedance spectroscopy (EIS) measurements were carried out for the working electrode in a frequency range of 10 mHz to 100 kHz at the open circuit potential with an amplitude of 5 mV. The EIS data were analyzed in the form of Nyquist plots. The cycling stability test was evaluated by GCD measurements at a current density of 5 A g^{-1} for 5000 cycles. The gravimetric specific capacitance of the electrodes based on the three-electrode system was calculated from the CV curves by Eq. (1):

$$C = \frac{1}{mv\Delta V}\int_{V_a}^{V_b} IVdV \quad (1)$$

Where C (F g^{-1}) represents the specific capacitance, m (g) is the mass of the active materials, v (mV s^{-1}) is the scan rate, and ΔV (V) refers to the range of potential window ($\Delta V = V_a - V_b$). The specific gravimetric capacitance can also be calculated from GCD curves

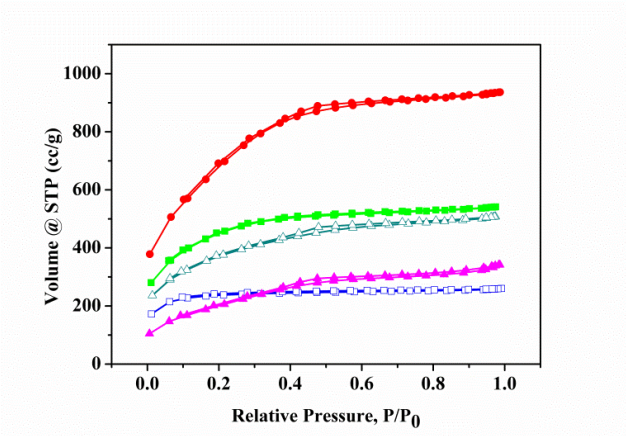

Fig. 2 N_2 adsorption isotherms at 77 K with different KOH/coal ratio □AC2T800t2, ■AC3T800t2, ●AC4T800t2, △AC5T800t2, ▲ AC6T800t2

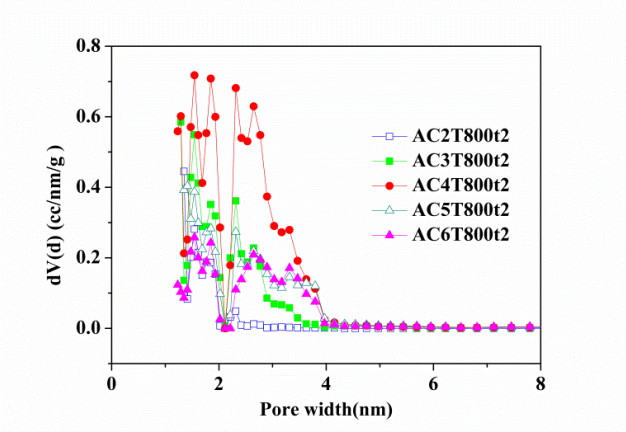

Fig. 3 Pore-size distribution curves for the ACs samples

according to Eq. (2):

$$C = \frac{I\Delta t}{m\Delta V} \quad (2)$$

Where I (A) refers to the discharge current, Δt (s) is the discharge time, and m (g) represents the mass of active material.

The CV and GCD curves were further measured using a two-electrode system in 6 M KOH. We chose the two electrodes with identical or very close weight for the measurements in the potential range of 0–1 V. The specific capacitance for the single electrode was obtained from the equation:

$$C = \frac{4I\Delta t}{m\Delta V} \quad (3)$$

Where m (g) is the total mass of active materials in both electrode. The energy density (E, W h kg^{-1}) of symmetrical supercapacitor system is calculated by using the following equation:

$$E = \frac{1}{2} C_t \Delta V^2 \quad (4)$$

Where C_t (F g^{-1}) is the gravimetric specific capacitance of the total symmetrical system. The power density (P, W kg^{-1}) is determined according to the equation:

$$P = \frac{E}{\Delta t} = \frac{I\Delta V}{m} \quad (5)$$

2.5 CO_2 sorption measurements

CO_2 sorption was measured through an equilibrium volumetric method similar to that previously described.[43-45] Approximately 1 g of the sample was used for each measurement. The cell sections were kept at 25 °C using an isothermal oven. As the CO_2 sorption proceeds, CO_2 was introduced into the sorption setup to produce an sorption isotherm under pressures up to 1 MPa. The equilibrium data were fitted by the Langmuir model. The form of the Langmuir equation is expressed as

$$\frac{n}{n_0} = \frac{bp}{1+bp} \quad (6)$$

Where n_0 (mmol g^{-1}) refers to the saturated adsorption capacity; p (MPa) is the equilibrium pressure; b (MPa^{-1}) is the Langmuir constant. Thus, n_0 and b are the adsorption parameters that are optimized from the least-squares criteria using the experimental data.

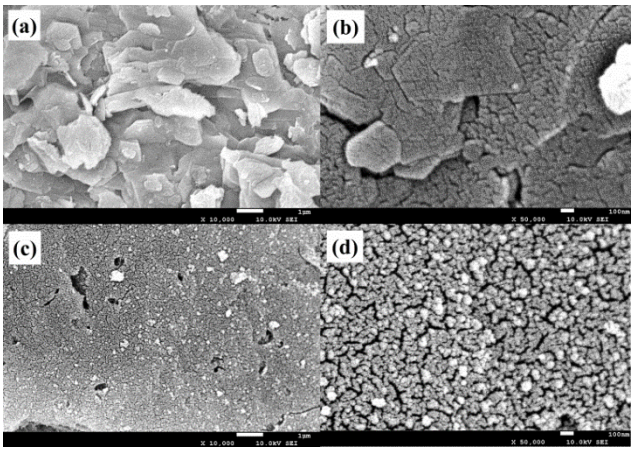

Fig. 4 SEM images of (a) (b) coal; (c) (d) AC4T800t2. Scale bars are 1 um for (a) (c) and 100 nm for (b) (d)

3. Results and discussion

3.1 Synthesis of High-surface-area Activated Carbons

The agent/coal ratio has been found to be the most important parameter in a chemical activation process.[20] In order to investigate the influence of KOH/coal ratio on the properties of final products, the KOH/coal ratio is varied in the range of 2-6 under the conditions of keeping the activation temperature at 800 °C and activation time at 2h.

The nitrogen adsorption isotherms of various samples at 77K are shown in Fig. 2. According to the International Union of Pure and Applied Chemistry (IUPAC) classification[46], all samples exhibit typical-I curves, demonstrating that they are mainly microporous materials.[47] Compared with other samples, AC4T800t2 displays the highest nitrogen adsorption capacity in the entire relative pressure region, which is attributed to its highest surface area. Fig. 3 displays the DFT pore size distribution from nitrogen adsorption. The ACs

Table 1 Influence of KOH/coal ratio on porous texture

Sample	Yield (%)	BET (m^2 g^{-1})	V_{mic} (cm^3 g^{-1})	V_t (cm^3 g^{-1})
AC2T800t2	50.79	711	0.3601	0.4023
AC3T800t2	46.03	1498	0.6554	0.8372
AC4T800t2	41.93	2457	0.9622	1.4480
AC5T800t2	35.98	1259	0.5384	0.7856
AC6T800t2	28.23	740	0.2841	0.5289

Keeping activation temperature at 800 °C and activation time at 2 h

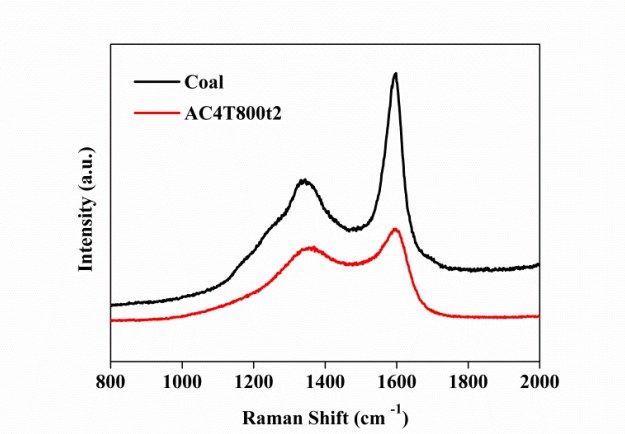

Fig.5 Raman spectra of Coal and AC4T800t2

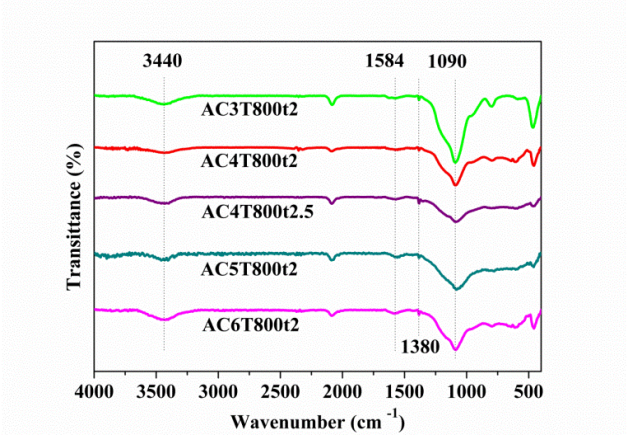

Fig. 7 FT-IR spectra of five ACs derived from coal

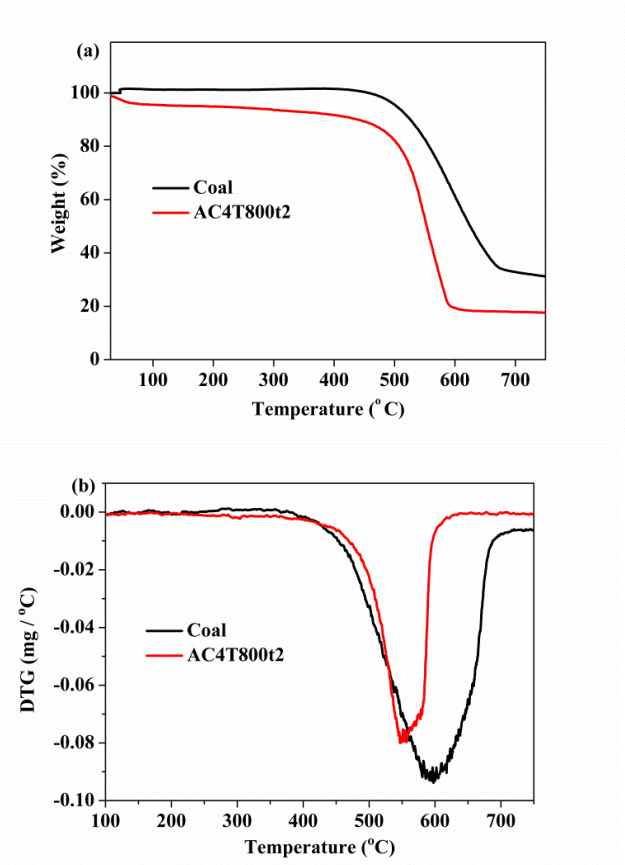

Fig. 6 TGA curves (a) and DTG curves (b) of Coal and AC4T800t2. The measurements were performed at the temperature range of 30–750 °C at a heating rate of 10 °C min^{-1} under the air atmosphere (20 mL min^{-1})

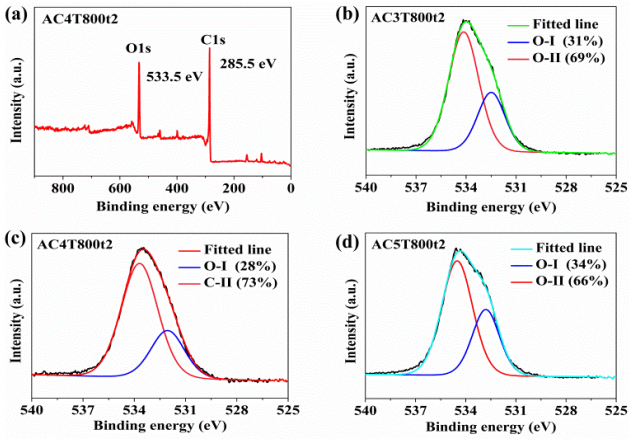

Fig. 8(a) XPS survey spectrum of AC4T800t2, (b-d) High-resolution XPS O 1s spectra of AC3T800t2, AC4T800t2, AC5T800t2

samples exhibit a narrow pore size distribution ranging from 1 to 4 nm. It has been confirmed that the existence of pore sizes ranging from micropore to mesoporosity, especially 2–5 nm is advantageous in improving the energy and power density of supercapacitor. In addition, micropores are critical for most of the energy storage in supercapacitors and CO_2 sorption. [9, 48] Therefore, the AC4T800t2 with high specific surface area and narrower pore size distribution could possess better electrochemical performance and CO_2 sorption property.

Table 1 summarizes the effect of KOH/coal ratio on the physical characteristic of ACs. This fact is shown in Fig. S2, where the BET surface area and yield is plotted versus KOH/coal ratio. It can be seen that the surface area and pore volume both increase with chemical ratio and reach the maximum for the KOH/coal ratio of 4. However, the yield of ACs continuously decreases with the increase of the KOH/coal ratio. Obviously, the pore texture of the ACs is significantly influenced by the KOH/coal ratios. The conclusion can also be proved by the SEM images (Fig. 4). As shown in Fig. 4, the original coal presents large thin sheets on the surface and has large irregular pieces, while the AC4T800t2 possesses relatively flat and smooth surfaces. Additionally, there are a lot of homogeneous small holes on the surface which are caused by KOH activation.

Raman spectroscopy is used to characterize the carbonaceous materials, particularly for distinguishing the ordered and disordered crystal structures, and the defect density of carbon materials.[25] In this study, it was used to characterize the change in the carbon textures after the activation by KOH (Fig. 5). Raman spectroscopy clearly shows the main D (1344 cm^{-1}) and G (1598 cm^{-1}) band peaks. The D-band reflects structural defects and amorphous carbon, while the G-band corresponds to the graphitic order.[31] The D- to G-band integrated intensity ratio (I_D/I_G) suggests the degree of the structural ordering with respect to a perfect graphitic structure.[49] Here, the D/G intensity ratios of coal and AC4T800t2 are determined to be 1.14 and 1.44, respectively, indicating that KOH activation brings about the decrease of the graphitization degree, which may be attributed to higher surface area and larger pore volume. The conclusion can be also proved by the thermo-gravimetric experiments (Fig. 6). From

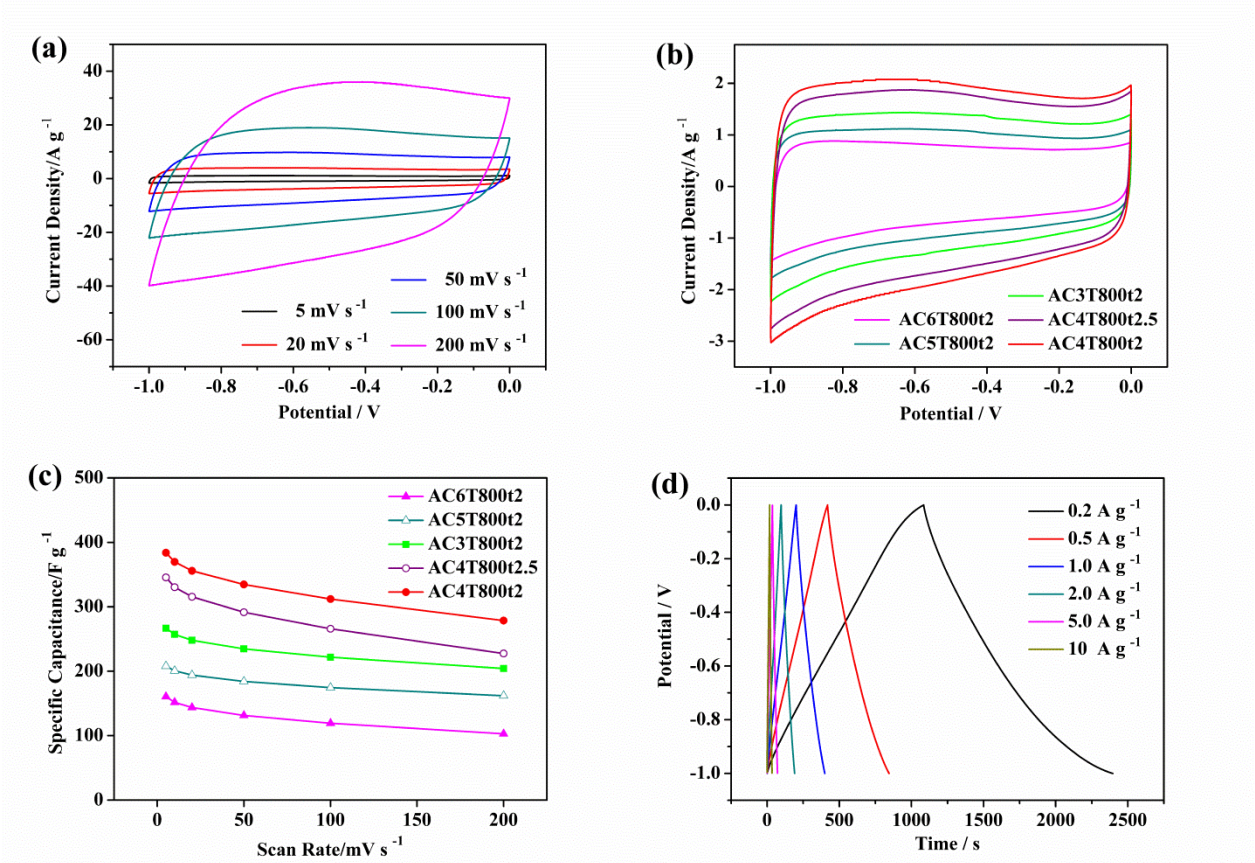

Fig. 9 (a) CV curves for the AC4T800t2 electrode in 6 M KOH at different scan rates from 5 to 200 mV s^{-1}, (b) CV curves of the ACs at 10 mV s^{-1}, (c) Rate performance of the ACs in the range of 5–200 mV s^{-1}, (d) Charge–discharge curves of the AC4T800t2 at different current density.

TGA curves (Fig. 6a), AC4T800t2 shows higher mass loss than coal. And there is no obvious weight loss for coal at 350-450 °C which could be attributed to the amorphous carbon burning.[36] DTG curves (Figure 6b) also show that the fastest weight loss rate of AC4T800t2 appears at the lower temperature than coal, which is consistent with the result of DTA curves (Fig. S4). In Fig. S4, the exothermic peak of AC4T800t2 rises at lower temperature. This may be explained: AC4T800t2 has higher surface area that can offer the larger number of active sites for O_2 or more oxygen-containing functional groups which could decompose of AC4T800t2 at the high temperature. Therefore, the thermal stability of AC in the air is worsened because of the activation of KOH, demonstrating that KOH activation lead to a poorer graphitized structure than coal.

The KOH-activation, therefore, could facilitate the synthesis of ACs with the enhanced surface area as well as the pore volume. Such an effect is ascribed to the partial gasification and the reaction of KOH and carbon.[50] The excess KOH will further burn off the carbon skeleton around micropores, resulting in the collapsed pore walls, and thus the surface area, pore volume and yield decrease substantially.[51] The mechanism of KOH activation is generally considered as a reaction between KOH and carbon: [52]

$$6KOH + 2C \rightarrow 2K + 3H_2 + 2K_2CO_3 \quad (7)$$

A generally accepted view is that KOH dehydrates to transform into K_2O at 400 °C; the resulting K_2O is reduced into metallic potassium by carbon at a high temperature and K is intercalated into the pseudographitic layers to develop a micropore structure.[53] K_2CO_3 begins to decompose into CO_2 and K_2O at temperature over 700 °C, and K_2O is also reduced to K.[54] With activation temperature increasing, the pores are further developed with the consumption of C, and the interconnected carbon walls are partly burnt out, which may be due to the further reaction between K_2O and C.

The activation time also plays an important role in the BET surface area and yield of ACs. Fig. S1 shows the nitrogen adsorption isotherms at 77K of ACs derived from different activation time. Details of pore characteristics of ACs at different activation time are given in Table S1. And Fig. S3 depicts the effect of activation time on the BET surface area and yield of ACs. The above results demonstrate that activation time do have much effect on the pore characteristics of AC products. The activation time of 2 h is found to be appropriate to reach the maximum of the BET surface area and total pore volume. In conclusion, S_{BET} and pore volume of the resultant ACs is significantly influenced by the KOH/coal ratio and activation time. Through the comparison of Fig. S2 and Fig. S3, it is apparent that the impact of KOH/coal ratio is stronger. The maximum specific area and pore volume of optimized sample (AC4T800t2) are 2457 $m^2 g^{-1}$ and 1.448 $cm^3 g^{-1}$, respectively.

Generally, the oxygen-containing functional groups can be formed by KOH activation. Furthermore, qualitative identification of surface functional groups was investigated by FT-IR spectroscopy over the range of 4000–400 cm^{-1} (Fig. 7). It is seen that all spectra are very similar. A band at 3440 cm^{-1} is assigned to the O-H stretching vibration. And the peaks at 1584, 1380 and 1090 cm^{-1} correspond to COO− anion stretching vibration, O-H bending vibration and C-O stretching vibration of ester respectively.[28, 31, 55, 56] From the above FT-IR analysis, it can be deduced that oxygen-containing groups may exist in the ACs, which can make effects on the electrochemical capacitive behaviors.[57] To further obtain more information regar-

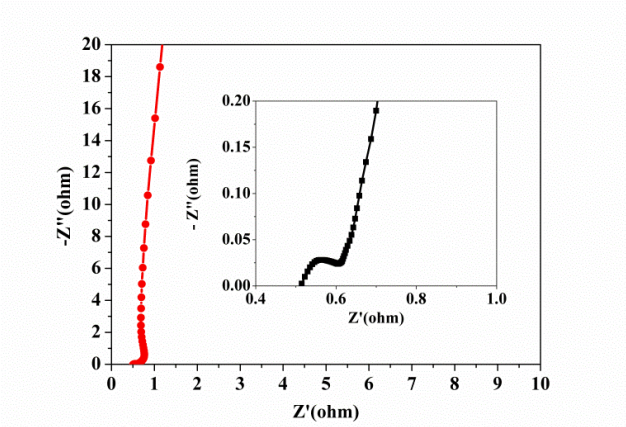

Fig. 10 Nyquist plot of the AC4T800t2 (inset enlarged high frequency region of Nyquist plot)

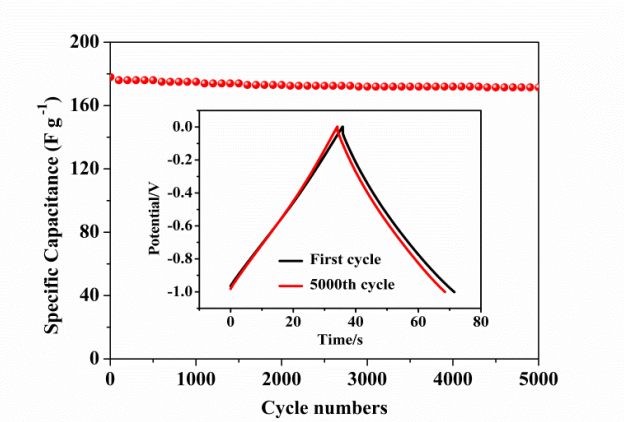

Fig. 11 Cycle-life of AC4T800t2 electrode at a constant current density of 5 A g^{-1} (inset: the charge–discharge curves of the first and 5000th cycle)

ding the chemical elements on the surface of ACs, XPS was performed on a representative samples. Fig. 8a shows the survey spectrum of AC4T800t2 within the range of 0–900 eV. Two strong peaks centered at binding energies of 285.5 eV and 531.9 eV, corresponding to C 1s and O 1s, respectively, suggesting the successful formation of oxygen-containing functional groups after the activation with KOH. The high-resolution O 1s spectra in Fig. 8(b-d) clearly reveals the existence two types of O functionalities: C–OH or C–O–C groups (O–I at 532.5 eV) and carboxylic groups (O-II at 534 eV).[27, 58] In all the ACs, O-II is the dominant functionalities.

3.2 Electrochemical Performance

To understand the electrochemical performance of the ACs as working electrodes, the electrochemical properties were evaluated in a 6 M KOH using a three electrode system. The CV curves of the AC4T800t2 electrode at varying scan rates from 5 to 200 mV s^{-1} (Fig. 9a) present a unique quasi-rectangular shape without any redox peaks, indicating an ideal double-layer capacitor nature of the charge–discharge process, and the electrode is stable in 6 M KOH aqueous electrolyte. [4, 31] The rectangular shape retains well even at the high scan rate of 200 mV s^{-1}, indicating desirable fast charge–discharge rates and low equivalent series resistance.[59]

As seen from Fig. 9b, the CV curve area of the AC4T800t2 electrode is much larger than other ACs electrode, illustrating that the AC4T800t2 offers a much larger capacitance, which is due to that AC4T800t2 possesses the higher SSA with abundant micropores (Table S2). The high surface area with abundant micropores can provide numerous active sides for electrolyte ion adsorption, and thus improves capacitive performance.[58] In addition, as seen from their CV plots, slightly polarization occurs on the positive and negative potential, which is attributed to a certain number of oxygen-containing functional groups on the ACs surface.[28]

Rate capability is a key factor for the application of carbon-based electrode materials. The relationships between specific capacitance calculated from the CV curves and the scan rates are summarized in Fig. 9c. The specific capacitance of ACs decreases with the increase of scan rates, which is related to diffusion limitation of the active ions in microporous structures.[47] To maintain the capacitance, more rapid electrolyte ionic mobility is required at higher scan rates; however, the microporosity of these materials limits their ionic mobility rates, thereby resulting in decrease of capacitance. A high specific capacitance of the optimal AC (AC4T800t2) is 384 F g^{-1} at the scan rate of 5 mV s^{-1}, with 73% retention even at a higher scan rate of 200 mV s^{-1}, implying a good rate performance. The result might be due to the mesopores formed in the carbon materials, which can facilitate the fast transfer and diffusion of electrolyte ions in the pore channels at high sweep rate, and thus enhance electrolyte accessibility to the microporous area.[49] The maximum specific capacitance of AC4T800t2 is as high as 384 F g^{-1} at a scan rate of 5 mV s^{-1},which is higher than the vast majority of AC materials with specific capacitance around 150-350 F g^{-1}.[48, 60]

In order to further investigate the performance of AC4T800t2, galvanostatic charge–discharge experiments were done at various current densities. In Fig. 9d, the AC4T800t2 possesses a typical triangular shape, indicating good capacitive properties, excellent conductivity.[49, 61]. And all discharge curves are almost symmetrical to the corresponding charge curves, indicating good electrochemical reversibility of this electrode.[62]

Electrochemical impedance spectroscopy (EIS) test was carried out in a frequency range from 10 mHz to 100 kHz in 6 M KOH solution. Fig. 10 shows the Nyquist plot (inset enlarged high frequency region of Nyquist plot) of the AC4T800t2. And the equivalent circuit for the fitting of the EIS data is achieved by ZsimpWin software. According to the equivalent circuit model[63] , the equivalent series resistance is as small as 0.6388 Ω for AC4T800t2, indicating high electronic conductivity in aqueous electrolytes. An almost vertical line suggests ideal double-layer capacitor behaviour at the low frequency region.[48, 49] The data in the middle frequency region reflect the diffusion of the electrolyte ions in the electrode pores with respect to Warburg impedance.[55] The insert in Fig. 10 displays a small semicircle at the high frequency region, reflecting the electrochemical reaction impedance of the electrode which is dependent on the electric conductivity and the porous structure of the active material.[64]

It is well accepted that the long-term cyclic stability is another important requirement for practical application of supercapacitors. Fig. 11 recorded the cycling stability data up to 5000 cycles for AC4T800t2 at a constant current density of 5 A g^{-1}. It shows only a slight drop of specific capacitance after the 5000 continuous cycles. The capacitance retains about 95% of the initial specific capacitance, indicating an extraordinary cycling performance. What's more, the 5000th galvanostatic charge–discharge curve (inset in Fig. 11) still displays a symmetrical triangular shape, demonstrating that the material possesses stable electrochemical performance and good charge propagation.[59]

In order to evaluate the electrochemical performance and the practical applications of the ACs for supercapacitor, a symmetrical two-electrode system was assembled with identical amount of active materials on both electrodes in 6 M KOH aqueous electrolyte. Fig.

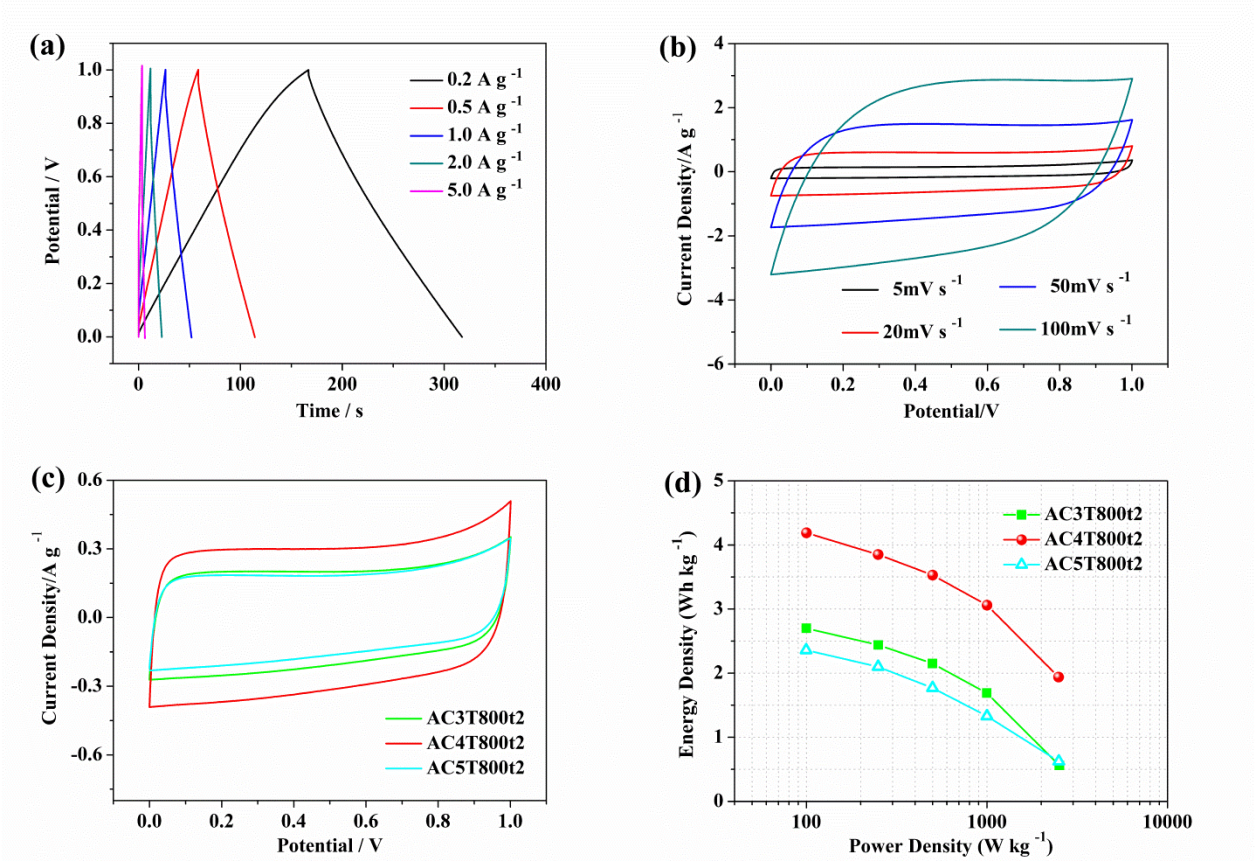

Fig.12 (a) Galvanostatic charge/discharge curves of the AC4T800t2 symmetric cell at various current densities, (b) CV curves of the AC4T800t2 symmetric cell at different scan rate, (c) CV curves of different AC symmetric cell at 10 mV s^{-1}, (d) Ragone plot of ACs tested by using a two-electrode symmetric supercapacitor in 6 M KOH aqueous electrolyte

12a records the GCD curves at different current densities in the voltage range 0–1 V. As presented in Fig. 12a, the linear and nearly symmetric charge/discharge curves reveal good supercapacitor behaviors.[65] The CV curves (Fig. 12b) of AC4T800t2 show quasi-rectangular shapes, suggesting a quick dynamics and good charge propagation[66], which is consistent with the results from the three-electrode system. In Fig. 12c, the CV curve of AC4T800t2 has a larger area than those of AC3T800t2 and AC5T800t2, indicating that AC4T800t2 possesses the higher specific capacitance and energy density, which can also be confirmed by Ragone curves in Fig. 12d. As depicted in the Ragone plot (Fig. 12d), normalized by the total mass of the active materials, the AC4T800t2 symmetric cell delivers a maximum energy density of 4.2 W h kg^{-1} with a powder density of 100 W kg^{-1} at the current density of 0.2 A g^{-1}.

3.3 CO_2 sorption properties

The CO_2 sorption isotherms measured at 298.15 K in pressure range of 0–1 MPa for AC samples are displayed in Figure 13. The CO_2 adsorption isotherms are Type I of IUPAC. The Langmuir model is used to fit the experimental data, and the fitting parameters of the Langmuir model are described in Table 2. The correlation coefficient is found to be above 0.99. Therefore, the Langmuir model is appropriate to fit the adsorption data, and provides good agreement with the experimental data. A higher value of n_0 indicates higher CO_2 adsorption capacity. The saturated sorption capacities (n_0) of the samples in our study varies from 6.10 to 20.81 mmol g^{-1} (26.84 wt% to 91.56 wt%). Among the samples, the AC4T800t2 possesses the highest CO_2 adsorption capacity and the AC2T800t2 sample possesses the lowest CO_2 adsorption capacity. Differences in SSA and pore volume can result in variation of CO_2 adsorption capacities. The higher surface area and the larger micropore volume offer more CO_2 physical adsorption sites, which account for higher CO_2 uptake.[67]

The linear relationship (correlation coefficient R^2 = 0.9958) between CO_2 sorption capacity at 1 MPa and BET specific surface area is presented in Figure. 14a. As a similar trend, CO_2 sorption capacity at 1 MPa also changes linearly with the micropore volume (correlation coefficient R^2 = 0.9714, Fig. 14b). This conclusion is consistent with previous researches.[67-69] It is revealed that better CO_2

Table 2 Textural parameters of ACs and sorption parameters of the Langmuir model

Sample	parameters of the Langmuir model			textural properties	
	n_0 (mmol/g)	b (MPa)	R^2	V_{mic} (cm^3/g)	S_{BET} (m^2/g)
AC2T800t2	6.10	1.1558	0.9995	0.2841	711
AC3T800t2	11.27	0.8555	0.9987	0.6554	1498
AC4T800t3	15.28	0.6900	0.9991	0.7364	1850
AC4T800t2.5	17.58	0.6855	0.9997	0.8414	2184
AC4T800t2	20.81	0.5741	0.9997	0.9622	2457

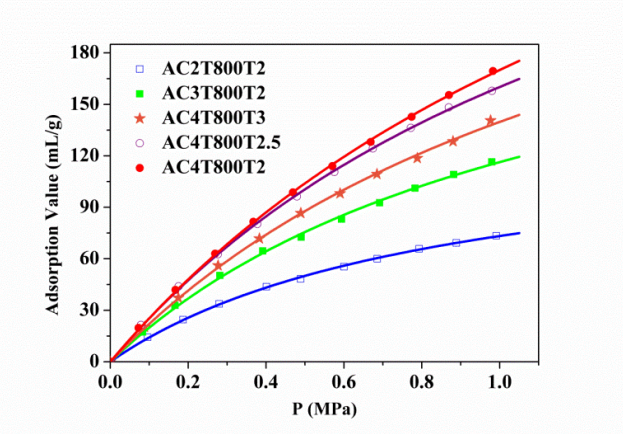

Fig. 13 CO_2 sorption isotherms for the ACs at 25 °C

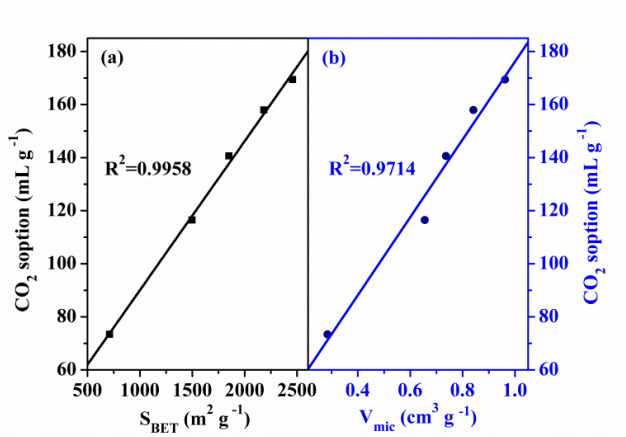

Fig. 14 CO_2 sorption capacity at 1MPa versus (a) specific surface area, (b) micropore volume

uptake is dependent on larger micropore volume and higher specific surface area.

The attractive forces at lower relative pressures is dominated by Van der Waals forces, while at higher relative pressures is dominated by capillary condensations.[45] The parameter b in Langmuir model describes the strength of interaction between adsorbate and adsorbent. In table 2, it can be observed that the value of b decreases with the increase of micropore volume. This is due to the fact that the capillary forces in the micropores can decrease the sorption rates[70], thus resulting in the weaker affinity of CO_2 toward the AC surface.

4. Conclusions

In summary, a facile and controllable one-pot synthesis of ACs was developed from cheap coal raw material. These ACs possessed high surface area and pore volume characteristic, leading to excellent performance as electrode materials for supercapacitors and as good absorbents for CO_2 capture. Notably, supercapacitors based on these AC electrodes in 6M KOH electrolyte solution exhibited high capacitance up to 384 F g^{-1} at the scan rate of 5mV s^{-1} and 279 F g^{-1} at 200 mV s^{-1}, which corresponds to 73% capacitance retention. These values are higher than the capacitance reported so far for many AC materials. Stable cycle performance was demonstrated, with 95% of the initial capacitance after 5000 cycles at the constant current density of 5 A g^{-1}. These superior performance features of ACs as electrodes for supercapacitors is mainly due to the high specific surface area associated with the narrow pore distribution as well as high electrical conductivity. Moreover, the CO_2 sorption capacities of the ACs were tested by volumetric method, and the adsorption data were fitted by the Langmuir model. AC4T800t2 exhibited high CO_2 sorption capacities reaching up to169.44 mL g^{-1} at 25 °C and 10 bar. There was a positive correlation between the CO_2 adsorption capacity and the SSA as well as the micropore volume.

Acknowledgements

This work was supported by the National Natural Science Foundation of China (201476145), & the National Basic Research Program of China (973 Program, 2011CB201202).

Notes and references

1 V. Sharma, A. Sahoo, Y. Sharma and P. Mohanty, *RSC Adv.*, 2015, **5**, 45749.
2 G. P. Hao, W. C. Li, D. Qian, G. H. Wang, W. P. Zhang, T. Zhang, A. Q. Wang, F. Schuth, H. J. Bongard and A. H. Lu, *Journal of the American Chemical Society*, 2011, **133**, 11378.
3 G. Park, *International Journal of Hydrogen Energy*, 2003, **28**, 645.
4 W. H. Qu, Y. Y. Xu, A. H. Lu, X. Q. Zhang and W. C. Li, *Bioresource technology*, 2015, **189**, 285.
5 C. Liang, Z. Li and S. Dai, *Angewandte Chemie*, 2008, **47**, 3696.
6 Y. Shi, Y. Wan and D. Zhao, *Chemical Society reviews*, 2011, **40**, 3854.
7 H. Nishihara and T. Kyotani, *Advanced materials*, 2012, **24**, 4473.
8 M. Sevilla and R. Mokaya, *Energy & Environmental Science*, 2014, **7**, 1250.
9 P. Simon and Y. Gogotsi, *Nature materials*, 2008, **7**, 845.
10 G. Dobele, T. Dizhbite, M. V. Gil, A. Volperts and T. A. Centeno, *Biomass and Bioenergy*, 2012, **46**, 145.
11 D. Adinata, W. M. Wan Daud and M. K. Aroua, *Bioresource technology*, 2007, **98**, 145.
12 J. Zhang, L. Jin, J. Cheng and H. Hu, *Carbon*, 2013, **55**, 221.
13 M. Yoshimune, T. Yamamoto, M. Nakaiwa and K. Haraya, *Carbon*, 2008, **46**, 1031.
14 J. Yang and K. Qiu, *Chemical Engineering Journal*, 2010, **165**, 209.
15 Y. Sudaryanto, S. B. Hartono, W. Irawaty, H. Hindarso and S. Ismadji, *Bioresource technology*, 2006, **97**, 734.
16 M. Wu, Q. Zha, J. Qiu, Y. Guo, H. Shang and A. Yuan, *Carbon*, 2004, **42**, 205.
17 M. A. Lillo-Rodenas, D. Cazorla-Amoros and A. Linares-Solano,*Carbon*, 2003, **41**, 267.
18 B. Xu, S. Hou, G. Cao, F. Wu and Y. Yang, *Journal of Materials Chemistry*, 2012, **22**, 19088.
19 J. Wang and S. Kaskel, *Journal of Materials Chemistry*, 2012, **22**, 23710.
20 D. Lozano-Castello, M. A. Lillo-Rodenas, D. Cazorla-Amoros and A. Linares-Solano, *Carbon*, 2001, **39**, 741.
21 M. Zhou, F. Pu, Z. Wang and S. Guan, *Carbon*, 2014, **68**, 185.
22 D. Prahas, Y. Kartika, N. Indraswati and S. Ismadji, *Chemical Engineering Journal*, 2008, **140**, 32.
23 M. A. Lillo-Rodenas, D. Lozano-Castello, D. Cazorla-Amoros and A. Linares-Solano, *Carbon*, 2001, **39**, 751.
24 Y. Zhai, Y. Dou, D. Zhao, P. F. Fulvio, R. T. Mayes and S. Dai, *Advanced materials*, 2011, **23**, 4828.

25 F. Zhou, Q. Liu, D. Kang, J. Gu, W. Zhang and D. Zhang, *Journal of Materials Chemistry A*, 2014, **2**, 3505.
26 Y. Gao, L. Li, Y. Jin, Y. Wang, C. Yuan, Y. Wei, G. Chen, J. Ge and H. Lu, *Applied Energy*, 2015, **153**, 41.
27 Z. Li, Z. Xu, H. Wang, J. Ding, B. Zahiri, C. M. B. Holt, X. Tan and D. Mitlin, *Energy & Environmental Science*, 2014, **7**, 1708.
28 C. Peng, X.-b. Yan, R.-t. Wang, J.-w. Lang, Y.-j. Ou and Q.-j. Xue, *Electrochimica Acta*, 2013, **87**, 401.
29 H. Pan, J. Li and Y. Feng, *Nanoscale research letters*, 2010, **5**, 654.
30 Y. Wang, Z. Q. Shi, Y. Huang, Y. F. Ma, C. Y. Wang, M. M. Chen and Y. S. Chen, *J Phys Chem C*, 2009, **113**, 13103.
31 Q. Liang, L. Ye, Z. H. Huang, Q. Xu, Y. Bai, F. Kang and Q. H. Yang, *Nanoscale*, 2014, **6**, 13831.
32 C. Merlet, B. Rotenberg, P. A. Madden, P. L. Taberna, P. Simon, Y. Gogotsi and M. Salanne, *Nature materials*, 2012, **11**, 306.
33 Y. Liang, Z. Li, X. Yang, R. Fu and D. Wu, *Chemical communications*, 2013, **49**, 9998.
34 M. R. Raupach, G. Marland, P. Ciais, C. Le Quere, J. G. Canadell, G. Klepper and C. B. Field, *Proceedings of the National Academy of Sciences of the United States of America*, 2007, **104**, 10288.
35 Q. Wang, J. Luo, Z. Zhong and A. Borgna, *Energy Environ. Sci.*, 2011, **4**, 42.
36 J. Hu, Z. Guo, W. Chu, L. Li and T. Lin, *Journal of Energy Chemistry*, 2015, **24**, 620.
37 V. Presser, J. McDonough, S.-H. Yeon and Y. Gogotsi, *Energy & Environmental Science*, 2011, **4**, 3059.
38 J. A. Delgado, M. A. Uguina, J. L. Sotelo, B. Ruíz and M. Rosário, *Journal of Natural Gas Chemistry*, 2007, **16**, 235.
39 M. Sevilla, J. B. Parra and A. B. Fuertes, *ACS applied materials & interfaces*, 2013, **5**, 6360.
40 M. S. Shafeeyan, W. M. A. W. Daud, A. Houshmand and A. Arami-Niya, *Applied Surface Science*, 2011, **257**, 3936.
41 R.-L. Tseng, F.-C. Wu and R.-S. Juang, *Separation and Purification Technology*, 2015, **140**, 53.
42 M. Sevilla and A. B. Fuertes, *Energy & Environmental Science*, 2011, **4**, 1765.
43 S. Hao, J. Wen, X. Yu and W. Chu, *Applied Surface Science*, 2013, **264**, 433.
44 J. Luo, Y. Liu, C. Jiang, W. Chu, W. Jie and H. Xie, *Journal of Chemical & Engineering Data*, 2011, **56**, 4919.
45 Y. Feng, W. Yang and W. Chu, *International Journal of Chemical Engineering*, 2014, **2014**, 1.
46 K. S. W. Sing, D. H. Everett, R. A. W. Haul, L. Moscou, R. A. Pierotti, J. Rouquerol and T. Siemieniewska, *Pure Appl Chem*, 1985, **57**, 603.
47 Q. Wang, W. Xia, W. Guo, L. An, D. Xia and R. Zou, *Chemistry - An Asian Journal*, 2013, **8**, 1879.
48 M. Biswal, A. Banerjee, M. Deo and S. Ogale, *Energy & Environmental Science*, 2013, **6**, 1249.
49 W. Qian, F. Sun, Y. Xu, L. Qiu, C. Liu, S. Wang and F. Yan, *Energy Environ. Sci.*, 2014, **7**, 379.
50 W. M. Qiao, S. H. Yoon and I. Mochida, *Energ Fuel*, 2006, **20**, 1680.
51 J. Pu, C. Li, L. Tang, T. Li, L. Ling, K. Zhang, Y. Xu, Q. Li and Y. Yao, *Carbon*, 2015, **94**, 650.
52 Y. S. Yun, S. Y. Cho, J. Shim, B. H. Kim, S.-J. Chang, S. J. Baek, Y. S. Huh, Y. Tak, Y. W. Park, S. Park and H.-J. Jin, *Advanced materials*, 2013, **25**, 1993.
53 S. H. Yoon, S. Lim, Y. Song, Y. Ota, W. M. Qiao, A. Tanaka and I. Mochida, *Carbon*, 2004, **42**, 1723.
54 X. Wei, S. Wan, X. Jiang, Z. Wang and S. Gao, *ACS applied materials & interfaces*, 2015, **7**, 22238.
54 M. Biswal, A. Banerjee, M. Deo and S. Ogale, *Energy & Environmental Science*, 2013, **6**, 1249.
55 X. Yan, J. Chen, J. Yang, Q. Xue and P. Miele, *ACS applied materials & interfaces*, 2010, **2**, 2521.
56 Y. Lv, L. Gan, M. Liu, W. Xiong, Z. Xu, D. Zhu and D. S. Wright, *J Power Sources*, 2012, **209**, 152.
57 C. T. Hsieh, W. Y. Chen and Y. S. Cheng, *Electrochimica Acta*, 2010, **55**, 5294.
58 L. Qie, W. Chen, H. Xu, X. Xiong, Y. Jiang, F. Zou, X. Hu, Y. Xin, Z. Zhang and Y. Huang, *Energy & Environmental Science*, 2013, **6**, 2497.
59 L.-F. Chen, Z.-H. Huang, H.-W. Liang, W.-T. Yao, Z.-Y. Yu and S.-H. Yu, *Energy & Environmental Science*, 2013, **6**, 3331.
60 L. L. Zhang and X. S. Zhao, *Chemical Society reviews*, 2009, **38**, 2520.
61 W. Huang, H. Zhang, Y. Huang, W. Wang and S. Wei, *Carbon*, 2011, **49**, 838.
62 G. Ma, Q. Yang, K. Sun, H. Peng, F. Ran, X. Zhao and Z. Lei, *Bioresource technology*, 2015, **197**, 137.
63 Y. Zhu, W. Chu, N. Wang, T. Lin, W. Yang, J. Wen and X. S. Zhao, *RSC Adv.*, 2015, **5**, 77958.
64 S. Zhao, C.-Y. Wang, M.-M. Chen, J. Wang and Z.-Q. Shi, *Journal of Physics and Chemistry of Solids*, 2009, **70**, 1256.
65 M. Wu, P. Li, Y. Li, J. Liu and Y. Wang, *RSC Adv.*, 2015, **5**, 16575
66 W. Qian, J. Zhu, Y. Zhang, X. Wu and F. Yan, Small, 2015, **11**, 4959.
67 L. Wan, J. Wang, C. Feng, Y. Sun and K. Li, Nanoscale, 2015, **7**, 6534.
68 J. Ludwinowicz and M. Jaroniec, Carbon, 2015, **94**, 673.
69 G. Sethia and A. Sayari, Carbon, 2015, **93**, 68.
70 S. Dutta, A. Bhaumik and K. C. W. Wu, Energy Environ. Sci., 2014, **7**, 3574.

Graphical abstract:

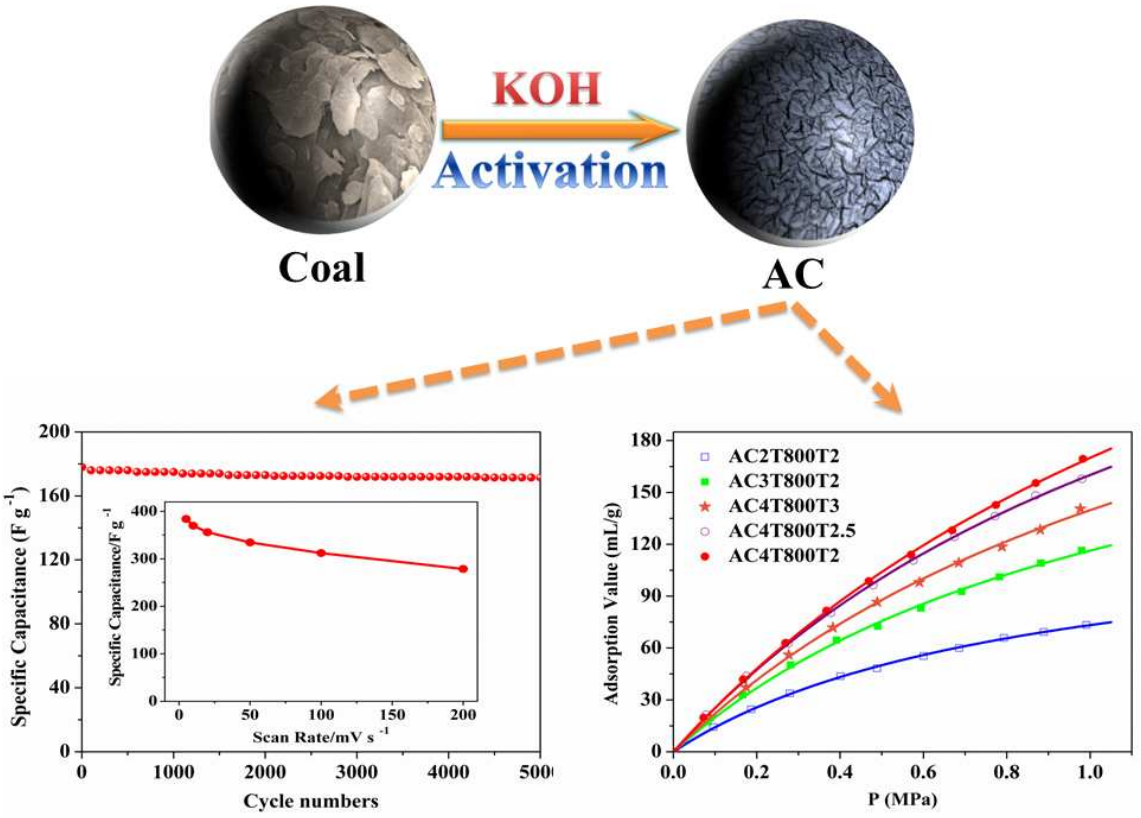

High performance activated carbons (ACs) were synthesized from cheap coal raw material via facile strategy by KOH activation. AC4T800t2 exhibited the higher BET surface area (2457 m^2 g^{-1}) and larger total pore volume (1.448 cm^3 g^{-1}) among the as-synthesized ACs samples. The optimized material (AC4T800t2) displayed the high specific capacitance (384 F g^{-1}) at the scan rate of 5 mV s^{-1}, good rate performance (73%) from 5 mV s^{-1} to 200 mV s^{-1}, excellent cyclic stability (95% retention capacity after 5000 cycles) at the current density of 5 A g^{-1} . AC4T800t2 also showed high CO_2 uptake of 169.44 mL g^{-1} (7.56 mmol g^{-1}) at 1 MPa.